Geological Society of America
Special Paper 358
2002

Estimation of the thermal structure of a young orogenic belt according to a model of whole-crust thickening

Teh-Ru Alex Song*
Kuo-Fong Ma
Institute of Geophysics, National Central University, Chung-Li, 320-54, Taiwan, Republic of China

ABSTRACT

A comprehensive understanding of the thermal properties beneath the Central Range of Taiwan is essential to decipher the process of mountain building and interpret the observed geophysical features, such as seismic velocity and seismicity. A first-order-approximation thermal model based on crustal thickening followed by constant erosion processes is described for the Central Range. The effect of groundwater circulation on the observed surface heat flow has been excluded in our evaluation. Our results indicate that crustal thickening causes a decrease in the geothermal gradient and the temperature. Erosion causes an increase in the geothermal gradient and the temperature. Through modeling, we derived the optimum geotherm below the Central Range by considering a thickening factor of 2 for crustal thickening occurring at 10 Ma following constant erosion since 5 Ma. The preferred final geotherm estimated a moderate geothermal gradient of ~17 °C/km and a temperature of ~210–550 °C at a depth of 10–30 km. The uncertainties in the thickening factor, the time of crustal thickening, and the prethickening crustal thickness have a temperature-difference effect of only a few tens of degrees compared to the temperature yielded by the preferred final geotherm. Other geotherm parameters such as radiogenic heat flow, scale depth, and surface heat production are also tested in the final geotherm calculations. Seismicity cutoff depth (i.e., the brittle-to-ductile transition depth) and seismic Q_p values set limits on the middle- and lower-crust temperatures determined by our model. The resulting moderate geothermal gradient differs from the notion that the crust beneath the Central Range is "hot," although the temperature in the shallow crust needs further investigation.

INTRODUCTION

Low seismic velocity and a lack of seismicity have been observed in the crust of several Cenozoic orogenic areas, such as the Alps (Meissner, 1986), Rocky Mountains (Prodehl and Pakiser, 1980), Himalaya (Mishra, 1982; Volvovsky et al., 1983), and Tibet (Rodgers and Schwartz, 1997). Similar phenomena from seismic tomography and local seismicity observations have also been revealed in Taiwan, a Cenozoic orogenic belt characterized by the collision between the Eurasian and Philippine Sea plates (Teng, 1990) (Fig. 1). Results of seismic tomography studies of Taiwan (Rau and Wu, 1995; Ma et al., 1996) indicate a low velocity in middle to lower crust beneath the Central Range. Figure 2 shows the tomographic P-wave

*Present address: Seismological Laboratory, California Institute of Technology, Pasadena, CA 91125

Song, T.A., and Ma, K.-F., 2002, Estimation of the thermal structure of a young orogenic belt according to a model of whole-crust thickening, *in* Byrne, T.B., and Liu, C.-S., eds., Geology and Geophysics of an Arc-Continent collision, Taiwan, Republic of China: Boulder, Colorado, Geological Society of America Special Paper 358, p. 121–136.

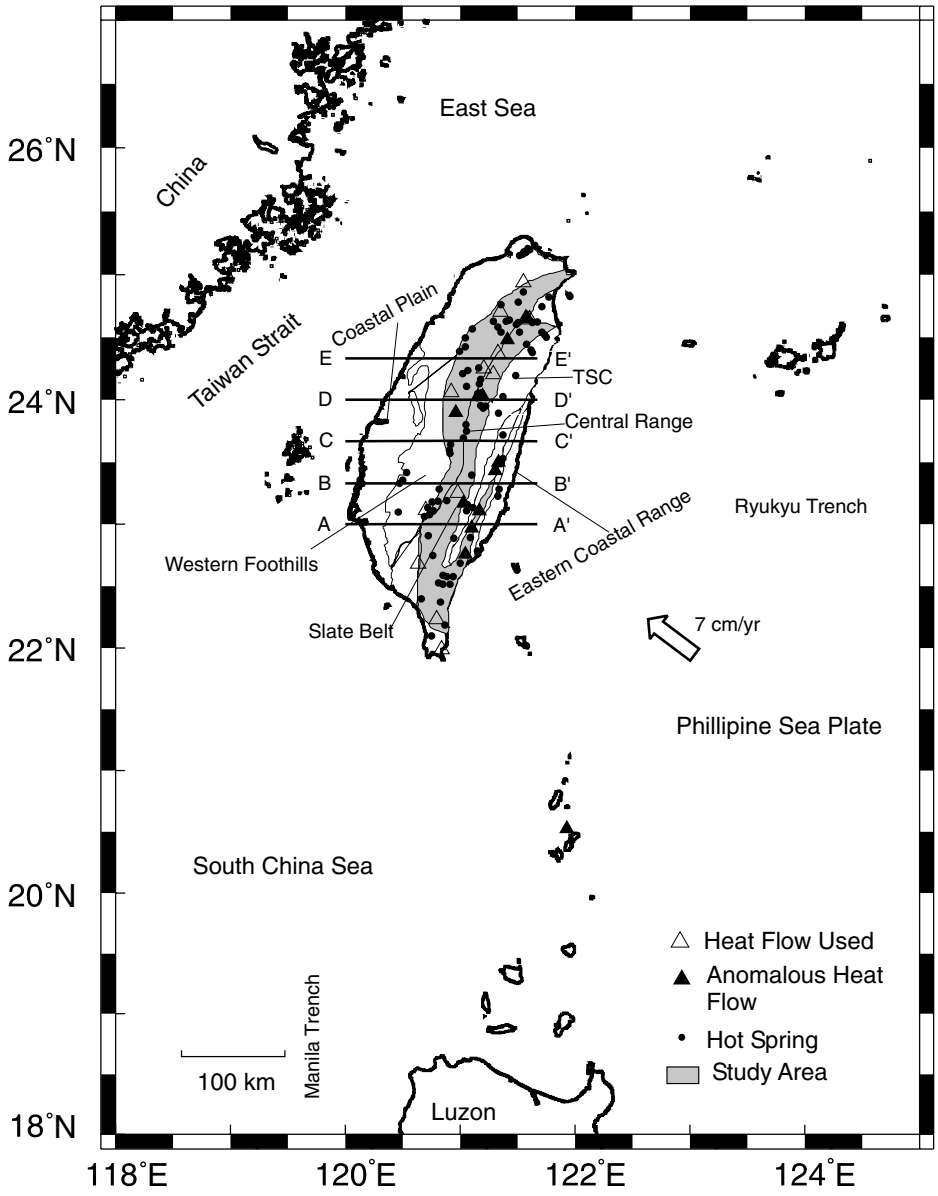

Figure 1. Geologic provinces, the metamorphic belt of Taiwan, and the distribution of heat flow (Lee and Cheng, 1986) used in the calculations (open triangles). The solid triangles indicate the abnormal heat flow of greater than 167 mW/m^2 or less than 33 mW/m^2. Solid circles represent the location of hot springs in Taiwan. Shaded area denotes the study area. A–A′ to E–E′ are the locations of profiles of seismicity and seismic P-wave velocity, as shown in Figure 2. TSC—Tananao Schist Complex.

velocity of Ma et al. (1996) with the background seismicity of $M > 3.0$ recorded from 1991 to 1998 by the Central Weather Bureau Seismic Network (CWBSN) of Taiwan along the profiles of A–A′ to E–E′ of Figure 1. Obvious low-velocity zones between the depths of 15 and 30 km were found in the profiles of A–A′ to E–E′; low rates of seismicity were also recognized in the profiles at these depths. The apparent low velocity and low seismicity in the middle and lower crust are commonly attributed to a high temperature and high geothermal gradient through those regions of the crust (Wu, 1978; Tsai, 1986; Wang et al. 1994; Wu et al. 1997). To decipher the possible significance of the seismic features, however, knowledge of the thermal structure is of fundamental importance.

The thermal structure in the Taiwan region had been investigated by Barr and Dahlen (1989) and Hwang and Wang (1993), respectively, to understand the mountain-building process in Taiwan. Barr and Dahlen (1989) considered a critical-wedge model to obtain the thermal structure of an actively deforming critically tapered fold-and-thrust belt (Suppe, 1980). Hwang and Wang (1993) analyzed the thermal evolution of Taiwan according to the model of discrete sequential thrusting. In these two studies, heat comes mainly from friction heating and shear-strain heating. Both groups used the observed heat-flow data in the Central Range (Lee and Cheng, 1986) to place constraints on their models. However, the resulting heat-flow values were anomalously high (>5 HFU) as the thermal evaluations did not account for the local groundwater-circulation effect. Lachenbruch and Sass (1977) and Lachenbruch et al. (1995) showed that the upward and downward circulation of groundwater could result in anomalously high and low surface

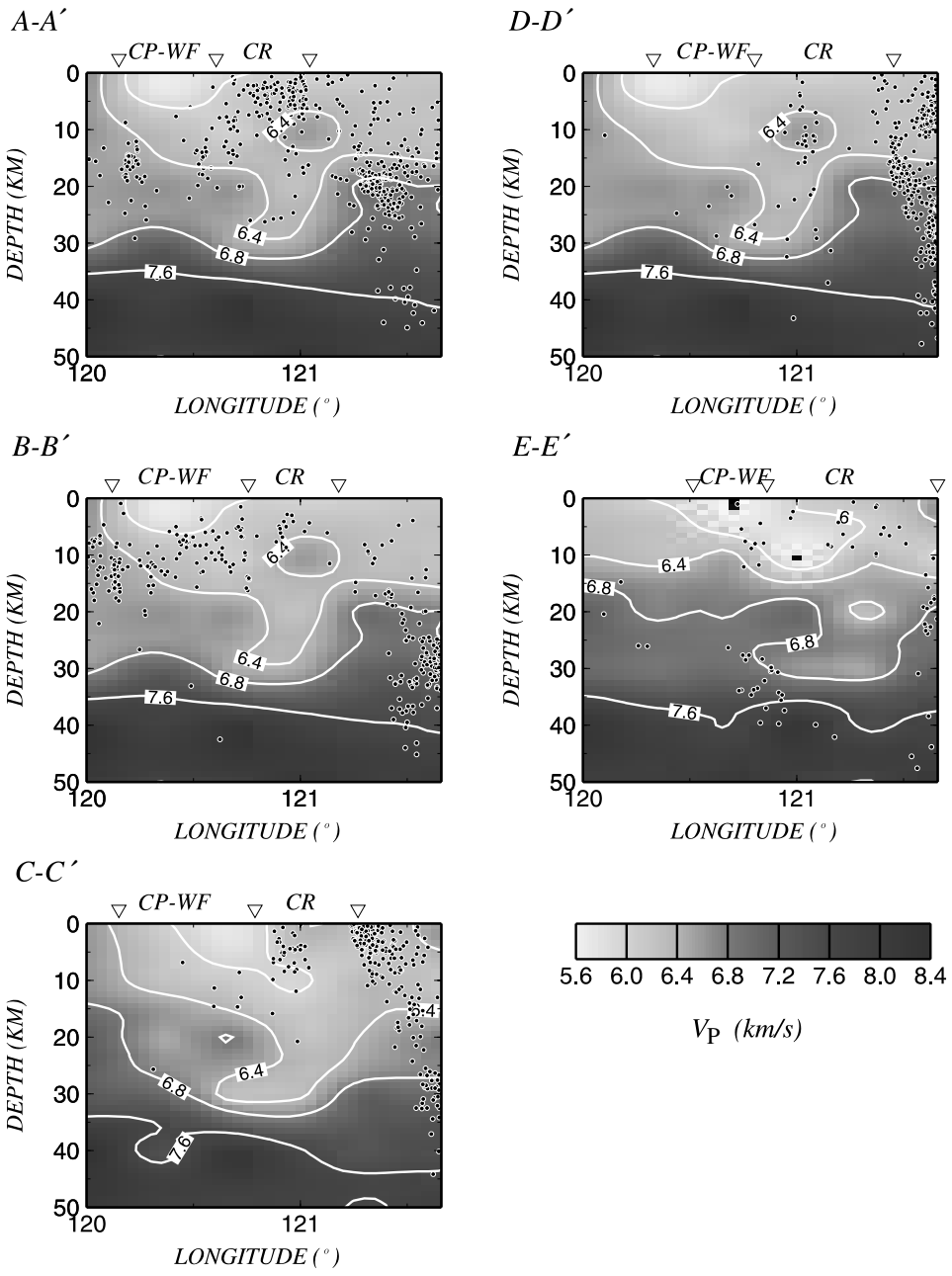

Figure 2. Seismicity and seismic P-wave velocity along profiles A–A′ to E–E′. Dots represent seismicity (M ≥ 3.0) recorded by the Central Weather Bureau Seismic Network in 1991–1998. Seismic velocity data are inferred from three-dimensional seismic tomography (Ma et al., 1996). CP-WF—Coastal Plain and Western Foothills, CR—Central Range.

heat-flow values. Lee and Cheng (1986) suggested that the anomalous surface heat flow observed in Taiwan (Fig. 1) is probably due to the groundwater circulation. Our groundwater-circulation simulation in this study supports this possibility. Thus, the use of the anomalously high surface heat flow as a constraint on the thermal-structure evaluation might not be appropriate.

In addition, both of these thermal models of Taiwan considered a contractional motion along a shallow décollement; this motion provided the frictional heating and internal strain heating for the deforming brittle wedge. However, several studies (England, 1978; Lachenbruch et al., 1995) have shown that the friction- and shear-strain heating might have only a small effect on the present-day heat flows within the possible lithospheric strength limitation of ∼1 kbar (Ord and Hobbs, 1989; Lamontagne and Ranalli, 1996). For this reason, we propose a crust-thickening model, which is considered appropriate for thermal modeling of Taiwan because it is the site of active arc-continent collision. However, the type of thickening is debatable; thickening values vary with different tectonic concepts (e.g., Toksoz and Bird, 1977; England and Thompson, 1984; Batt and Braun, 1997). Our geotherm evaluation supports the model of whole-crust thickening, suggested by England and Thompson (1984).

Evaluation of geotherms is difficult in an orogenic belt, because the crustal deformation and the associated thermal evolution are not steady, but rather time dependent. In this study, we quantitatively evaluate the first-order thermal properties beneath the Central Range of Taiwan. A model involving whole-crust thickening is considered to satisfy the regional average surface heat flow, excluding the anomalously high and low values. Other minor heat sources, such as frictional heating, metamorphic heating, shear-strain heating, and heterogeneous thermal conductivity are neglected in our first-order approximation. It must be noted that our model is not sensitive to the geothermal gradient and temperature in the shallow crust (<10 km) because of the assumption of constant erosion rate. Horizontal heat advection caused by horizontal motion is also not considered in our calculations. Several synthetic tests on thermal parameters are conducted to justify our calculations.

GEOLOGIC SETTINGS

Taiwan is situated on the eastern margin of the Eurasian continent and is the consequence of an arc-continent collision between the Eurasian and Philippine Sea plates (Fig. 1). Radiometric dating indicates that the onset of the Cenozoic orogeny in Taiwan was at ca. 10–12 Ma (e.g., Lan et al., 1990; Lo and Yui, 1996). From basin sedimentary-sequence analysis (Teng, 1990), the relevant collision may have begun at 5 Ma. The degree of deformation increases eastward from the Coastal Plain through the Western Foothills, to the Central Range. These three areas represent, respectively, the undisturbed region and the fold-and-thrust belt and metamorphic core formed in the Taiwan orogeny. The Central Range, situated in the center of the Taiwan orogenic belt, has existed since middle Miocene time (Ho, 1982, 1988). The Central Range mainly consists of metamorphic terranes including the Slate Belt geologic province and the Tananao Schist Complex (Fig. 1). The Slate Belt consists of slates, argillites, and phyllites. The predominant constituents in the Tananao Schist Complex are green schists, black schists, and some minor gneisses. From west to east in the Central Range, the metamorphic facies increase from zeolite, prehnite-pumpellyite, to greenschist; amphibolite facies is finally reached in the northeastern part of the Central Range. High exhumation rates are not uncommon in the Central Range, especially in the region of the Tananao Schist Complex (Liu, 1982, 1988), according to analyses of fission-track data. Tsao (1996) showed that the exhumation rate has varied and has increased from the west to the east, on the basis of illite crystallinity, zircon fission-track ages, and K-Ar ages of metamorphic terranes in the Central Range, excluding the data related to faulting. Because of the abundance of faults and fractures, hot springs are well distributed in the Central Range (Chen, 1989) (Fig. 1). Owing to the complex structure in the Central Range, the thermal properties in the middle and lower crust are still under investigation. Because the thermal history of the Tananao Schist Complex in the Central Range is very complicated (Lan et al., 1990), in this study, we concentrate on resolving the thermal structure of the Slate Belt in the Central Range. The geotherm parameters used in our model therefore correspond to the Slate Belt region in the Central Range.

GEOTHERMAL ESTIMATIONS

In this study, we have tried to incorporate all of the available data related to the geothermal structure to obtain a first-order approximation of the regional average thermal structure beneath the Central Range of Taiwan. The present regional average thermal structure, in our model, is mainly controlled by three factors: (1) heat flow from the mantle, (2) the decay of radiogenic elements in the continental crust, and (3) the geotherm perturbation from crustal thickening, uplift, and erosion. The first two and the last factors represent the steady and transient factors, respectively.

The steady factor

As long as the tectonic environment is stable, only the radiogenic heat flow (Q_A)- and mantle heat flow (Q_L) will contribute to the surface heat flow (Q_0) (England and Richardson, 1980), i.e., $Q_0 = Q_L + Q_A$ (all Q terms are in units of mW/m^2). The radiogenic heat flow is related to the amount of radiogenic heat produced and its depth distribution. The surface radiogenic heat production (A_0, in μW/m^3), which is related to the crustal content of potassium (K), thorium (Th), and uranium (U), can be evaluated from

$$A_0 = \rho \times 10^{-2} \times (3.48[\mathrm{K}] + 2.56[\mathrm{Th}] + 9.52[\mathrm{U}]), \quad (1)$$

where ρ is the density in kg/m^3, [K] is the K concentration in %, and [Th] and [U] are the Th and U concentrations in ppm (Rybach and Cermak, 1982). The heat production usually decays exponentially with depth in the form of $A(z) = A_0 \exp(-z/D)$, where $A(z)$ is the heat production at the depth z and D is the scale depth, which represents the depth at which the radiogenic heat production decays to $1/e$ of the surface radiogenic heat production. This exponential decay is due to a decrease in the abundance of the radiogenic elements with depth (Lachenbruch, 1970).

The nonradiogenic heat flow corresponds, in general, to the mantle heat flow in stable provinces (England and Richardson, 1980; Sclater et al., 1980; Morgan and Gosnold, 1989; Artemieva and Mooney, 2001). In this case, the geotherm in steady state could be calculated by

$$T(z) = \frac{Q_L}{k} z + \frac{D^2}{k} A_0 (1 - e^{-z/D}), \quad (2)$$

for a one-dimensional regional average approximation (Lachenbruch, 1970), where $T(z)$ represents the temperature in °C at

depth z, k is the thermal conductivity, D is the scale depth, and Q_L is the mantle heat flow from radioisotopes in the mantle and core.

The transient factors

If thickening, uplift, and erosion take place, time-dependent thermal perturbations will be recognized (e.g., Stuwe et al., 1994; Mancktelow and Graseman, 1997). In Taiwan, various orogenic models have been proposed by different groups (Teng, 1990; Lu and Hsu, 1992; Hsu and Sibuet, 1995; Wu et al., 1997; Hwang et al., 1997). However, which model is most appropriate is still under debate. In addition, the effect of the Taiwan orogeny on the lithospheric mantle is not well resolved. England and Thompson (1984) proposed a whole-crust homogeneous-thickening model for the active collisional environment of Taiwan. This model may be appropriate to use in investigating the regional thermal structure in the Taiwan orogenic belt. The model considers orogeny as due to a rapid phase of crustal thickening, during which little temperature change occurs in individual rocks, followed by erosion. The crustal thickening is assumed to occur by homogeneous horizontal shortening of the entire crust. The geothermal gradient below the crust is not affected by the thickening crust. In this case, the temperature perturbation (ΔT) due to crustal thickening can be estimated, for $z < f \times H$, as

$$\Delta T = -\frac{\pi}{4}[1 + (l - fH)/l] \left[\frac{A_0 D e^{-1}(f^2 - 1)}{2k} + \frac{Q_L H(f - 1)}{k}\right], \quad (3a)$$

(modified from England and Thompson, 1984), where f is the thickening factor, l is the lithosphere thickness, and H is the crustal thickness before thickening. When $z > f \times H$, the temperature perturbation should be represented as

$$\Delta T = -\frac{\pi}{4}(1 + (l - fH)/l) \left[\frac{A_0\, De^{-1}(f^2 - 1)}{2k} + \frac{Q_L H(f - 1)}{k}\right] \times (l - z)/(f \times H) \quad (3b)$$

ΔT represents the mean thermal perturbation between the surface and the base of the lithosphere when crustal thickening is complete. Equation 3 could express the thermal perturbation caused by the crustal thickening and the altering of heat production. The perturbed temperature was distributed in the lithosphere as a periodic cosine function that decays exponentially with time as

$$\Delta T(z, t) = \Delta T \cos\frac{\pi Z}{2l} \exp\left[\frac{-\pi^2 \kappa t}{4l^2}\right], \quad (4)$$

where κ is the thermal diffusivity. $\Delta T(z,t)$ represents the geothermal perturbation at depth z after crustal thickening for time t. $\square T(z,t)$ is mainly dependent on the thickening factor (f), lithosphere thickness (l), and prethickening crust thickness (H).

When the crust undergoes tectonic uplift and erosion, these processes will lead to thermal advection and result in erosion-caused heat flow (Q_E), which contributes an increase of nonradiogenic heat flow. For a constant erosion rate, the erosion heat flow can be written as

$$Q_E(\lambda) = k\left.\frac{\partial T}{\partial T}\right|_{t=t_1} [1 + 4p^2 - 4i^2\mathrm{erfc}(p)]; \quad (5a)$$

where

$$p = \frac{H_E}{2\sqrt{\kappa\lambda}}, \quad (5b)$$

from England and Richardson (1980), where H_E is the erosion thickness, λ represents the duration from the initiation of erosion to the present time (called the "erosion time period" hereafter), and i^2 erfc represents the repeated integrals of the error function, and $\left.\frac{\partial T}{\partial Z}\right|_{t=t_1}$ is the average thermal gradient above H_E at the time t_1 when the erosion had just been initiated. Erosion would cause not only heat-flow increase but also reduction of radiogenic heat production. The surface heat production A_0 and surface heat production before erosion $A_0(\lambda)$ has the relationship as

$$A_0 = A_0(\lambda)\exp(-H_E/D), \quad (6)$$

where H is the initial crust thickness before the onset of thickening. If we assumed that the crustal thickening occurred at time t_0 and that the erosion occurred at time t_1, the geotherm at time t_f due to crustal thickening and erosion can be written as

$$T(z, t_f) = \frac{Q_r}{k}z + \frac{D^2}{k}A_0(t_f - t_1)[1 - e^{-z/D}] + \Delta T(z, t_f - t_0), \quad (7)$$

where $T(z,t_f)$ represents the geotherm at time t_f, $A_0(t_f - t_1)$ is the surface heat production before erosion, and the reduced heat flow (Q_r) is now the combination of mantle heat flow (Q_L) and erosion heat flow (Q_E) for the erosion time period $\lambda = t_f - t_1$; therefore, $Q_r = Q_L + Q_E(\lambda)$.

Determination of geotherm parameters

Table 1 lists the geotherm parameters used in our calculation. However, several geotherm parameters are not available as they are difficult to obtain in the Central Range. Some arguments related to these geotherm parameters are addressed

next. The sensitivities of the geotherm evaluation to these geotherm parameters are examined later.

Surface heat flow, Q_0. The distribution of the observed surface heat-flow data in the Central Range (Lee and Cheng, 1986) is shown in Figure 1. Lee and Cheng (1986) suggested that the observed anomalously high (>167 mW/m^2) and low heat-flow values (<33 mW/m^2) might be caused by groundwater circulation. Excluding the anomalously high and low heat-flow values, the average heat-flow value in the Central Range will be about $Q_0 = 97 \pm 32$ mW/m^2. To examine this hypothesis, we simulated the groundwater circulation to see its effect on the surface heat flows.

Lachenbruch and Sass (1977) showed that the surface heat flow at a local site will increase or decrease with the upward or downward movement of groundwater. The disturbance (ΔQ) in surface heat flow due to the moving groundwater can be represented by

$$\Delta Q = Q_0[e^{\pm(h/s)} - 1], \quad (8)$$

where h is the depth of circulating groundwater, $s = \alpha/V$ is the characteristic length scale for groundwater circulation, where $\alpha(\sim 18.96$ m^2/yr) is thermal diffusivity of water and V is velocity of the groundwater. The positive and negative signs of (h/s) indicate the upward and downward movement of groundwater, respectively. Chen (1989) suggested that the depth of groundwater circulation beneath the Central Range is ~ 4 km, which is comparable with the general observations (Elder, 1965; Lachenbruch and Sass, 1977). Because the velocity of groundwater is not well known in Taiwan, we used various V values in the calculations for a simple idealized one-dimensional model of groundwater circulation (see Appendix). After the calculations, we consider $V = 0.0075$ m/yr to be the velocity of groundwater circulation in the current study. For the circulated depth of 4 km, this velocity of groundwater circulation will require 130 000 yr (the stabilization time) to achieve equilibrium, which is most comparable to the common observation of stabilization time of 10^5 yr for $h = 4$ km (Elder, 1965).

TABLE 1. PARAMETERS USED IN THE GEOTHERMAL CALCULATION

Thermal conductivity, k	2.5 mW/m^2
Present heat production, A_0	1.711 μW/m^3
Mantle heat flow, Q_L	27 mW/m^2, 38 mW/m^2
Scale depth, D	7 km, 11 km
Thermal diffusivity, κ	1.5×10^{-6}m^2/s
Crustal thickness, H	30 km
Lithospheric thickness, l	100 km
Surface heat flow, Q_0	97 ± 32 mW/m^2
Radiogenic heat flow, Q_A	39 ± 13 mW/m^2
Erosion thickness, H_E	8.2 km, 8 km
Heat production before erosion, $A_0(\lambda)$	5.52 μW/m^3, 3.56 μW/m^3
Thickening factor, f	2
Erosion heat flow, Q_E*	22.57 mW/m^2

*Q_E estimated for $Q_L = 38$ mW/m^2, $D = 7$ km, and $\lambda = 5$ Ma. Other estimations are listed in Table 3.

The corresponding characteristic length, s, of the groundwater circulation with the velocity of 0.0075 m/yr is ~ 2528 m. Considering $Q_0 = 97 \pm 32$ mW/m^2, $h = 4$ km, and $s = 2528$ m, from Equation 8, we obtain anomalously high heat-flow values of ~ 250 to 500 mW/m^2 and anomalously low heat-flow values of ~ 10 to 30 mW/m^2 due to the upward and downward movement of groundwater circulation, respectively. Figure 3 shows that the observed anomalous heat-flow values are compatible with our estimation. The plot suggests that the measured high and low heat-flow values in the Central Range mentioned by Lee and Cheng (1986) probably result from groundwater circulation. These anomalous heat-flow data, thus, are excluded from our thermal modeling. It would not be adequate to take these values as constraints in thermal-structure evaluation.

Radiogenic heat flow, Q_A. It is apparent that the radiogenic heat production should be reduced by the erosion process, while the augmentation caused by the crustal-thickening mechanism would yield an increase of crust materials. Thus, describing the radiogenic heat flow from orogenic crust is rather complicated. Huerta et al. (1996, 1998) attempted to explain the thermal structure as a response of accretion, erosion, and radiogenic heating. They mainly considered the trade-offs among erosion rate, accretion velocity, and the heat production of those accreted materials to the thermal structure. A higher accretion rate and a lower erosion rate accompanying high heat-production material would result in higher temperature (~ 500 °C) at the depths of 20–30 km. However, determination of such parameters and their mutual effects on the geotherm beneath Taiwan are rather difficult because of the lack of data. Thus, for the estimation of radiogenic heat flow, we adopt the global average value as $\sim 40\%$ of surface heat flow (i.e., $Q_A = 0.40Q_0$). This relationship has been shown to be suitable regardless of the age of geologic provinces (Pollack and Chapman, 1977; England and Richardson, 1980; Vitorello and Pollack, 1980). It implies that the radiogenic heat flow increases in proportion to the surface heat flow owing to the augmentation of heat production during the orogenic process. Considering this approximation, we estimated the radiogenic heat flow to be $\sim 39 \pm 13$ mW/m^2 in the Central Range. However, other approximations of 35% and 45% of the surface heat flow as being due to radiogenic heat flow are also considered later to examine their effect on the final geotherm evaluation.

Mantle heat flow, Q_L. Sclater et al. (1980) considered that the reduced heat flow (Q_r) usually increases with transient heat flow and then decays over geologic time; Q_r reaches a constant heat flow of ~ 21–27 mW/m^2 as the background mantle heat flow. England and Richardson (1980) obtained the reduced heat flow of ~ 38 m/Wm^2 for Precambrian shields; this value is treated here as the background mantle heat flow. Because the mantle heat flow in Taiwan is not available, we use the value of 27 mW/m^2 and 38 mW/m^2 as the background mantle heat flow in our calculation. The effect of the uncertainty on the mantle heat flow is discussed in the next section.

Scale depth, D. Scale depth usually can be estimated from

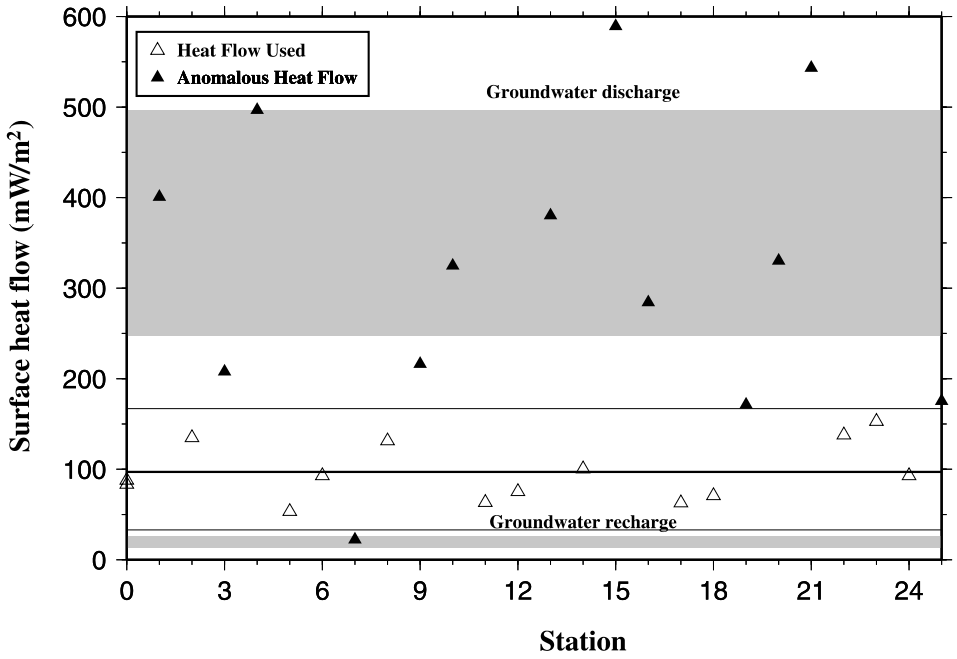

Figure 3. The range of calculated anomalous heat flows due to groundwater recharge (lower shaded region) and discharge (upper shaded region) compared with the observed anomalous heat flows (solid triangles) of greater than 167 mW/m^2 and less than 33 mW/m^2, suggested by Lee and Cheng (1986). Heat-flow values used in this study are shown by open triangles. Two thin solid lines are the heat flows of 167 mW/m^2 and 33 mW/m^2. Thick solid line represents the mean surface heat flow.

the observed surface heat flow (Q_0) and surface radiogenic heat production (A_0) as $Q_0 = Q_r + A_0D$ (Lachenbruch, 1970). After analyzing the heat-flow and production pairs reported in the global data, we concluded that the scale depth does not vary significantly among different geologic province (Vitorello and Pollack, 1980; Sclater et al., 1980; Haack, 1983). It is generally within 5–15 km. Because there is no observation of a pair of heat-flow and heat-production values in Taiwan, in this study, we adopt the scale depths of 7 and 11 km from Vitorello and Pollack (1980). The effect of the uncertainty of the scale depth is also discussed in the next section.

Erosion thickness, H_E, and heat production before erosion, $A_0(\lambda)$. The heat production usually decays exponentially with depth owing to the decrease in the radiogenic elements in the rocks, but the production also can be treated as constant within the crust. Chang (1989) surveyed the Central Range and compiled the amount of radiogenic elements in different lithologies. Table 2 shows the amount of radiogenic elements in different lithologies and their corresponding heat production. Radiogenic heat production varies with lithologies and decreases with the increase in the grade of metamorphism, in other words, it decreases with depth. Thus, the assumption that heat production decreases exponentially with depth might be more appropriate than constant heat production. Given that the metamorphic belts of Taiwan consist of about two-thirds slate and one-third phyllite, A_0 could be estimated at $\sim$1.711 μW/m^3. The present surficial radiogenic heat production (A_0) would have been buried at the depth z in the past before erosion and uplift (Vitorello and Pollack, 1980). If the crust is eroded by H_E during the erosion time period λ, the heat production before erosion, $A_0(\lambda)$, thus, can be estimated as $A_0(\square) = A_0\exp(H_E/D)$. Considering the reduced radiogenic heat flow due to the occurrence of erosion, the erosion thickness can be estimated as

$$H_E = D\ln\left[\frac{DA_0\exp(-H/D) - Q_A}{DA_0}\right], \qquad (9)$$

For crustal thickness $H = 30$ km and radiogenic heat flow = 39 mW/m^2, we estimate the erosion thickness $H_E = \sim$8.2 km and 8 km for the scale depths of 7 km and 11 km, respectively. According to the estimation of H_E, we can obtain $A_0(\lambda)$ values of 5.52 μW/m^3 and 3.56 μW/m^3 for $H_E = 8.2$ and 8 km, respectively. From sediment-accumulation analysis and radiometric dating complied by Teng (1990), the estimated erosion thickness is $\sim$8 km and the exhumation of rock is $\sim$10 km. Given the elevation of 1–4 km in the Central Range and H_E = 8 km, our calculations yield the exhumation depth of $\sim$9–12 km, which is compatible with the geologic evidence.

Thickening factor, f. The thickening factor indicates the ratio of the crustal thickness after and before crustal thickening. In the Taiwan orogenic belt, the prethickening crustal thickness could be reasonably postulated as 30 km, which is about the crustal thickness of the undisturbed Coastal Plain on the western side of Taiwan derived from P_n-wave study (Ma and Song, 1997), reflection experiments (Shih et al., 1998), and

TABLE 2. THE CONTENT OF RADIOGENIC ELEMENTS IN SURFACE METAMORPHIC ROCKS IN THE CENTRAL RANGE

Metamorphic Rocks	K (%)	U (ppm)	Th (ppm)	Density (kg/m³)	Radiogenic heat production (μW/m³)
Phyllite	3.13	2.81	16.3	2400	1.905
Slate	2.80	2.62	13.5	2400	1.662
Black schist	2.96	2.47	13.4	2400	1.637
Green schist	1.07	0.43	1.62	2400	0.287
Gneiss	1.90	1.85	9.70	2700	1.325

ray-tracing methods (Lee, 1999). The crustal thickness in the Central Range is ~45 km according to the P_n study of Ma and Song (1997). Therefore, it could be reasonable to consider the thickening factor as at least 1.5. Taking 9–12 km to be the amount of rock exhumation, as derived in the previous paragraph, the thickening factor becomes ~2. We take the thickening factor of 2 in our geotherm evaluation. Other thickening factors such as 1.5 and 2.5 are also tested later to justify the effects of the thickening factor on the geotherm estimation.

Time of thickening t_0 and time of erosion t_1 vs. erosion heat flow, Q_E. According to geologic and geochronologic data (Teng, 1990; Chen and Wang, 1995; Tsao, 1996), the collisional process in Taiwan is thought to have initiated at ca. 12–10 Ma. This time range is derived from the time of metamorphism, the direction change of plate motion, and sediment sequence analysis. We consider the time of deep burial metamorphism of 10 Ma (Tsao, 1996) as the initiation of crustal thickening in our thermal model. The time of initiation of erosion was estimated from the sediment-accumulation analysis in the Western Foothills and the Coastal Range (on the east side of Taiwan) (Teng, 1990). The relevant onset of erosion ought to be 5–3 Ma. Although there is no direct evidence to indicate when the erosion starts after crustal thickening, the delay between crustal thickening and erosion might be related to the density increase at the bottom of the crust from the granulite to eclogite transition (Richardson and England, 1979). Because the timing of initiation of erosion is sensitive to erosion heat flow (Q_E), we calculated the corresponding erosion heat flow for the erosion time period λ = 10 Ma, 5 Ma, and 3 Ma. By using the average surface heat flow as a constraint and considering the factor R,

$$R = \frac{Q_A + Q_L + Q_E(\lambda)}{Q_0} - 1 \times 100\%, \qquad (10)$$

we can estimate the optimized erosion time period λ in our calculation. The factor R indicates the compatibility between the sum of estimated Q_A, Q_L, and Q_E values and the observed surface heat flow. The smaller the absolute value of R ($|R|$), the more compatible the calculated results to the observed heat flow.

RESULTS AND DISCUSSION

Geotherm evolution

After detailed discussions about the determination of geotherm parameters, the estimated geotherms and their variation due to crustal thickening and erosion are shown in Figure 4. For convenience, we use letters to denote the calculations using pairs of Q_L and D values as follows: (A) Q_L = 27 mW/m² and D = 7 km, (B) Q_L = 27 mW/m² and D = 11 km, (C) Q_L = 38 mW/m² and D = 11 km, and (D) Q_L = 38 mW/m² and D = 11 km. Hereafter, we refer to these pairs of Q_L and D values as A, B, C, and D, respectively. Figure 4A shows the postulated initial geotherms before thickening. The geothermal gradient in the middle and lower crust (10–30 km) is ~15 ± 2 °C/km. The corresponding temperatures range from 250 ± 50 to 550 ± 100 °C. Figure 4B represents the corresponding geotherms accompanied by crustal thickening. The effect of crustal thickening reduces the temperature by ~150–200 °C at the depth of 25 km and reduces the average geothermal gradient to ~8 ± 2 °C/km in the depth range of 10–30 km.

Table 3 lists the factor R calculated for Q_L and D pairs A to D and for λ = 3 Ma, 5 Ma, and 10 Ma. The corresponding erosion heat flows and their contributions to the surface heat flow are also listed in Table 3. It is obvious that the effect due to the variations of scale depth on the estimation of erosion heat flow is less than that caused by variations in the mantle heat flow. The most important factor in evaluating the erosion heat flow is λ. Among these calculations, the one based on C for λ = 5 Ma shows results that are the most comparable to the observed values with R = 2.73%. The calculation based on C for λ = 5 Ma generates an erosion heat flow of ~22.57 mW/m², which contributes ~23.4% to the observed average heat flow. Other calculations using A (for λ = 3 Ma) and D (for λ = 10 Ma) also produce heat-flow values similar to the observed surface heat flow ($|R|$ = ~5%). Figure 4C depicts the geotherms for different time intervals of erosion for the optimum calculation using C (for λ = 5 Ma), A (for λ = 10 Ma), and D (for λ = 3 Ma), respectively. The geotherm estimated from the optimum calculation using C is thus considered as the final preferred geotherm. The geotherms of the latter two calculations can be treated as the deviated ranges of the geotherm. The final preferred geotherm shows that the temperature increases by ~200 °C at the depth of 25 km after thickening and erosion as shown in Figure 4C.

In general, the geotherm perturbations from crustal thickening and erosion are compensated for during the relative short relaxation time within 10 m.y. The final preferred geotherm has a geothermal gradient of ~17 °C/km in the depth range of 10–30 km. The geothermal gradient ranges at the depths of deviated

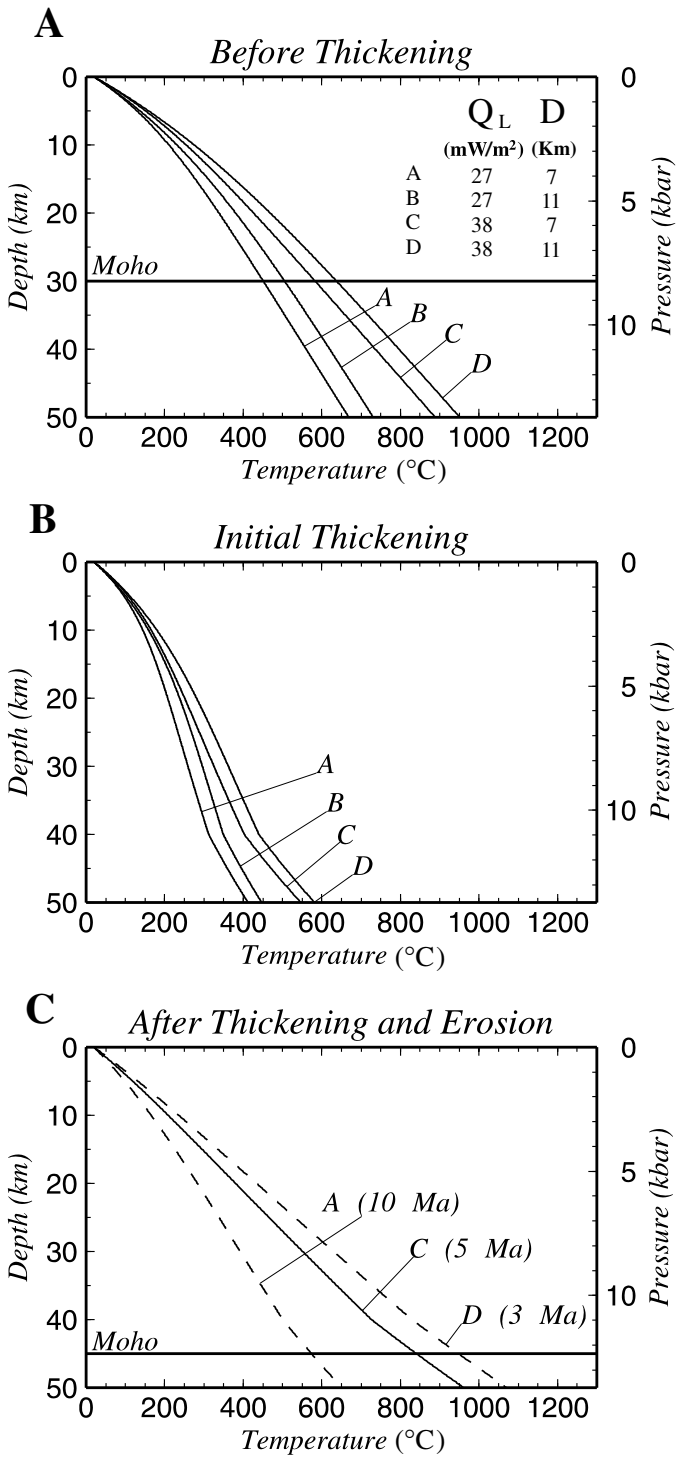

Figure 4. Average geotherm obtained considering three different parameters: (A) The radioactive heat production and mantle heat flow for different combinations of mantle heat flows (Q_L) and scale depths (D). (B) The crustal-thickening effect. (C) After thickening and erosion, the final preferred average geotherm was calculated by using the Q_L and D pair C (see text) for $\lambda = 5$ Ma. The results of calculations using Q_L and D pairs A (10 Ma) and D (3 Ma) are also shown for comparison (dashed lines).

from 11 to 20 °C/km at the depths of 10 km, 20 km, and 30 km are ~170–240 °C/km, 275–425 °C/km, and 390–630 °C/km, respectively. The effect of the uncertainty in the mantle heat flow (27 mW/m^2 or 38 mW/m^2) on the estimation of the geotherm, as compared in calculations using Q_L and D pairs A and C (Fig. 4C), results in an erosion time period uncertainty of ~2 m.y. and a temperature uncertainty of ~100 °C at the Moho (45 km).

Sensitivity test of geotherm parameters

Because the geotherm parameters used in our calculations are based on several assumptions, the uncertainties in our modeling caused by these assumptions are examined to justify our results.

First, we examine the effects of the thickening factor (f), the time of crustal thickening (t_0), and the prethickening crustal thickness (H) on the thermal perturbation due to crustal thickening because they are prior information for the calculation of the geotherm. Therefore, $f = 1.5$, 2, and 2.5, $t_0 = 8$ Ma, 10 Ma, and 12 Ma, and $H = 25$ km, 30 km, and 35 km are all simulated. On the basis of the equations 3 and 4, the thermal perturbations from the alternative 27 sets of thermal parameters are derived and shown in Figure 5. Comparing the thermal perturbations to the results of the preferred final geotherm calculation, where $f = 2.0$, $H = 30$ km, and $t_0 = 10$ Ma, the effect of changing the thickening factor (f) is seen to be the most significant. However, the effect of the ± 0.5 difference in the thickening factor on the geotherm is only ~30 °C at the depth of 10 km and 60 °C at the depth of 30 km. The variation of crustal thickness yields a temperature difference of ~10 °C. As to the time of crustal thickening, it merely affects the temperature by ~5 °C for the relevant, short period since crustal thickening. Therefore, the uncertainties in the thickening parameter in our evaluation might not be significant to our result.

Second, we examine other geotherm parameters, such as present radiogenic heat flow (Q_A), scale depth (D), and present surface heat production (A_0). They are all closely related to the final geotherm. These parameters affect the estimation of the erosion thickness (H_E), initial surface radiogenic heat production ($A_0(\lambda)$), prethickening geotherm, and final geotherm. The estimation of erosion thickness would affect the evaluation of erosion heat flow and the final result as well. Besides using the radiogenic heat-flow value of 40% of surface heat flow (39 mW/m^2), radiogenic heat flows of 35% (34 mW/m^2) and 45% (44 mW/m^2) of surface heat flow are taken into consideration. In addition, D values of 5 km, 10 km, and 15 km and A_0 values of 1.0 □W/m^3, 1.5 □W/m^3, and 2.0 □W/m^3 are also considered in our calculations. Table 4 lists the estimations of erosion thickness (H_E) and initial surface heat production ($A_0(\lambda)$) from the various combinations of Q_A, D, and A_0. Smaller A_0 and larger D values would result in larger H_E values, but smaller $A_0(\lambda)$ values. Both $A_0(\lambda)$ and H_E increase with Q_A. For the same A_0 and D, Q_A will cause about 0.5–1.5 km and 0.3–1.0 μW/m^3

TABLE 3. EROSION HEAT FLOWS (Q_E)

	Q_L (mW/m²)	D (km)	λ = 3 Ma			λ = 5 Ma			λ = 10 Ma		
			Q_E (mW/m²)	Q_E/Q_0 (%)	R (%)	Q_E (mW/m²)	Q_E/Q_0 (%)	R (%)	Q_E (mW/m²)	Q_E/Q_0 (%)	R (%)
A	27	7	35.24	36.50	+4.46	19.37	20.06	−11.97	11.90	12.33	−19.71
B	27	11	38.25	39.69	+7.58	21.57	22.34	−9.70	13.06	13.53	−18.51
C	38	7	41.12	42.59	+21.83	22.57	23.38	+2.73	13.80	14.29	−6.34
D	38	11	44.02	45.59	+24.95	24.78	25.67	+5.02	14.94	15.47	−5.17

Note: The erosion heat flows (Q_E) were obtained by considering different combinations of mantle heat flow (Q_L) and scale depths (D) for erosion time periods of λ = 3 Ma, λ = 5 Ma, and λ = 10 Ma, respectively.

uncertainty in H_E and $A_0(\lambda)$, respectively. On the basis of the parameters in Table 4, the estimation of the prethickening geotherm could be derived as depicted in Figure 6. Several estimations shown in this figure are comparable even with different combinations of these thermal parameters. Compared with the previous preferred geotherm calculation in which D = 7 km or 11 km and A_0 = 1.711 μW/m^3, most estimations of the prethickening geotherm deviate from the results of previous calculations using Q_L and D pairs A–D by ~50 °C at 30 km. Overall, thermal parameters as surface heat production ($A_0(\lambda)$), scale depth (D), erosion thickness (H_E), radiogenic heat flow (Q_A), erosion time (λ), and mantle heat flow (Q_L) are included in the final geotherm calculation. We first exclude those estimations of H_E (<8 km) and $A_0(\lambda)$ (>6 μW/m^3) in Table 4 that are incompatible with common observations (Teng, 1990; Rudnick, 1992); then we combine different values for mantle heat flow and erosion time period, and finally we obtain 72 sets of geotherm evaluations. By using the criterion |R| as defined in the previous section, we obtain 12 possible geotherms with |R| <5%. The results are shown in Figure 7. The 12 possible final geotherms are almost within our previous calculations using Q_L and D pairs A–D. Although there are uncertainties regarding those critical thermal parameters, synthetic tests confirm that our results are robust. In the following, we discuss the correlation between our result and other independent constraints, such as seismic attenuation Q_p, the maximum depth of seismicity, and geologic evidence.

Seismic Q_p values set limits on deep-crustal temperature

For another independent seismic constraint, in this paper we consider the relationship between seismic anelasticity and temperature. The laboratory measurements on anelasticity of dry peridotite have shown that the seismic attenuation of compressional waves (Q_p^{-1}) depends on the ratio of temperature to the solidus temperature (T_m) as

$$Q_p/Q_{pm} = \exp[g(T_m/T - a)], \quad (11)$$

where Q_{pm} is the Q_p value at the solidus temperature T_m and T is the temperature (in kelvins). The constants g and a are 13.3 and 1.03 for $T_m/T > 1.08$. Q_{pm} is a linear function of pressure (Sato and Sacks, 1989):

$$Q_{pm} = Q_0 + P/P_0, \quad (12)$$

where P is the pressure and Q_0 and P_0 are 3.5 and 73 MPa, respectively. From the solidus of dry peridotite (Takahashi, 1986), the relationship between T and Q_p can be extrapolated to mantle depth. Once Q_p is derived, we can estimate temperature by equations 11 and 12. Chen et al. (1996) selected only high-quality data, employed a spectral decay method, and determined a three-dimensional Q_p structure of the Taiwan region to the depth of 100 km. According to the estimated average Q_p value in the Central Range, we infer its corresponding T_Q (temperature estimated from seismic Q_p) to compare with our final geotherm. Because the relationship of Q_p and T is limited to the upper mantle owing to the available laboratory measurements of peridotite, we only compare our result with T_Q at the depth of the upper mantle. The dry and wet solidus values for T_m had been determined by Sato (1994); we estimate the T_Q for dry and wet mantle, respectively. The estimated average Q_p at the depth of 35–50 km is ~610 from Chen et al. (1996). This Q_p value yields T_Q values of ~892 °C and 675 °C for dry and wet mantle, respectively. The temperature T_Q is approximately within the range of our geotherm evaluation, as depicted in Figure 8.

Seismicity cutoff depth sets limit on middle-crustal temperature

Actually, seismicity cutoff depth has been treated as a geothermometer in the crust (Doser and Kanamori, 1986; Bordi and Iizuka, 1993). It can be used to examine the temperature versus earthquake cutoff depth relationship (Sibson, 1982). If the seismicity cutoff depth (brittle-to-ductile transition) is determined, its corresponding temperature could be obtained. On the basis of this method, Song (1997) has shown that the temperatures related to the earthquake cutoff depths are ~270–400 °C and 350–510 °C, at depths of 15 km and 25 km, respectively. As depicted in Figure 8, these temperatures are also comparable with our estimated geotherm.

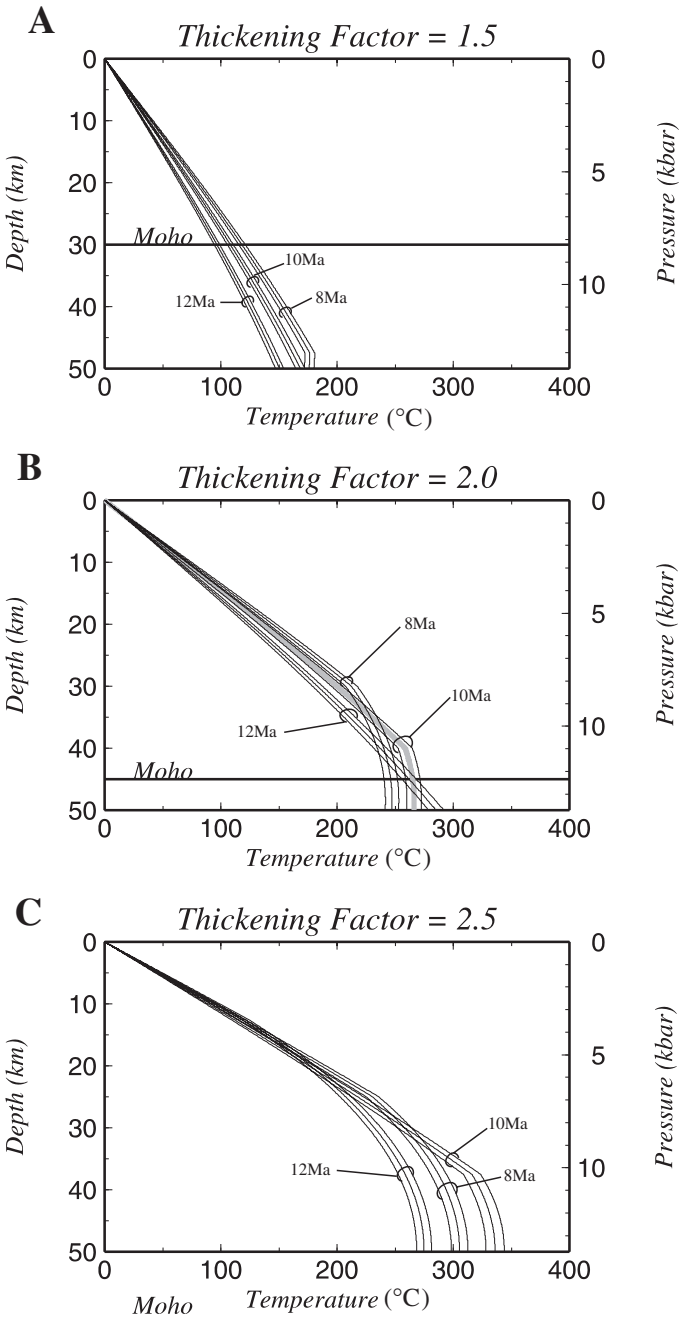

Figure 5. Results of thermal-parameter sensitivity test on whole-crust homogeneous thickening. Thickening times of 12 Ma, 10 Ma, and 8 Ma and prethickening crustal thicknesses of 25 km, 30 km, and 35 km are introduced in the test. The three lines in each thickening time correspond to the prethickening crustal thicknesses of 25 km, 30 km, and 35 km from left to right, respectively. (A) Temperature reduction with thickening factor of 1.5. (B) Temperature reduction with thickening factor of 2. (C) Temperature reduction with thickening factor of 2.5. The thick gray line in B represents the crustal-thickening effect considered in this study.

TABLE 4. THE EROSION THICKNESS

A_0 (μW/m^3)	D	Q_A = 35% of Q_0		Q_A = 40% of Q_0		Q_A = 45% of Q_0	
		$A_0(\lambda)$ (μW/m^3)	H_E (km)	A_0 (λ)	H_E (μW/m^3)	$A_0(\lambda)$ (μW/m^3)	H_E (km)
1.0	5	6.68	9.5	7.69	10.2	8.67	10.8
1.0	10	3.42	12.3	3.90	13.6	4.35	14.7
1.0	15	2.38	13.0	2.68	14.8	3.00	16.5
1.5	5	6.77	7.5	7.58	8.1	8.55	8.7
1.5	10	3.44	8.3	3.92	9.6	4.37	10.7
1.5	15	2.44	7.3	2.77	9.2	3.08	10.8
1.71*	7*			5.52	8.1		
1.71*	11*			3.56	8.0		
2.0	5	6.77	6.1	7.63	6.7	8.61	7.3
2.0	10	3.46	5.5	3.95	6.8	4.41	7.9
2.0	15	2.51	3.4	2.83	5.2	3.15	6.8

Note: The erosion thickness (H_E) and $A_0(\lambda)$ were derived from a combination of different scale depths (D) and present surface heat production A_0, Q_A and Q_0 are in units of mW/m^2.
The parameters used in our study.

TABLE 5. THE THERMAL PARAMETERS USED IN FINAL 12 POSSIBLE GEOTHERMS

No.	A (μW/m^3)	D (km)	Q_A (mW/m^2)	Q_L (mW/m^2)	λ (Ma)
1	1.0	10	44	27	10
2	1.5	10	44	27	10
3	1.0	10	34	38	10
4	1.5	10	39	38	10
5	2.0	10	44	38	10
6	1.0	10	34	27	3
7	1.5	10	39	27	3
8	2.0	10	44	27	3
9	1.0	10	39	27	5
10	1.5	10	44	27	5
11	2.0	10	44	27	5
12	1.5	10	39	38	5

Geology and geochronology set limits on shallow-crustal temperature

Before comparing with the geologic evidence, it should be mentioned that the crustal heterogeneity is dramatic, especially in shallow crust. The exhumation rate, generally, is not constant though it is proportional to the metamorphic grade (Tsao, 1996). Therefore, our one-dimensional thermal model could not reflect this lateral variation, but only represent the average geotherm. Because of the complex thermal history in the Tananao Schist Complex (Lan et al., 1990; Lo and Yui, 1996), we do not attempt to discuss its thermal state. As mentioned previously, considering the amount of erosion and the topography of the Central Range, rocks beneath the Central Range might have been exhumed by 9–12 km. The metamorphic temperature and pressure are ~200–330 °C at 1–3 kbar in the Central Range (Chen and Wang, 1995), as depicted by the shaded box in Figure 8. After evaluating the possible geotherm in the Central Range, we calculate the corresponding pressure-temperature-time (*P-T-t*) path for rocks originally buried at 9 km (rock A) and 12 km (rock B) and exhumed at a constant rate, from our

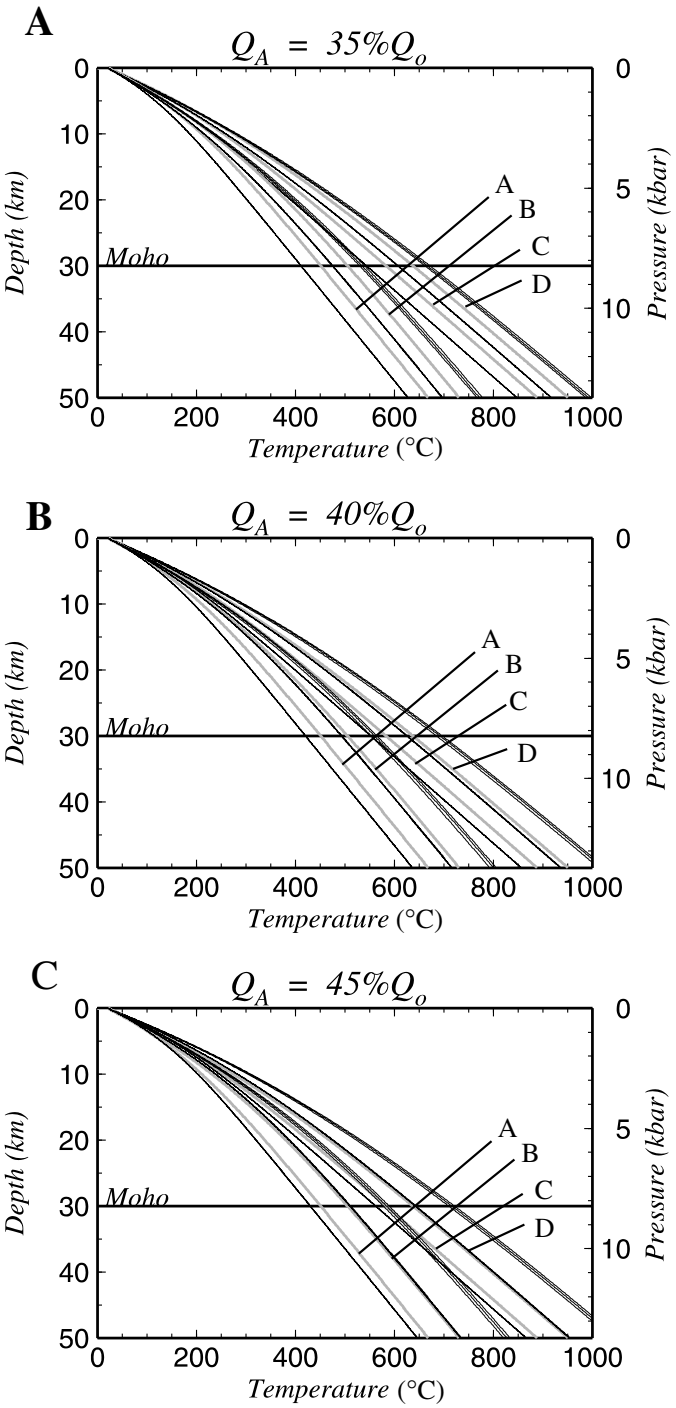

Figure 6. Prethickening geotherms (solid lines) calculated from the parameters used in Table 4 for the combination of A_0 values of 1.0 μW/m^3, 1.5 μW/m^3, 2.0 μW/m^3, and D values of 5 km, 10 km, and 15 km. Prethickening crustal thickness is 30 km. Results in (A), (B) and (C) represent the estimations with radiogenic heat flows of 35%Q_0, 40%Q_0, and 45%Q_0, respectively. Mantle heat flows of 27 mW/m^2 and 38 mW/m^2 are also involved in the calculation. The prethickening of geotherms Q_L and *D* pairs A–D used in our study are shown by gray lines for comparison.

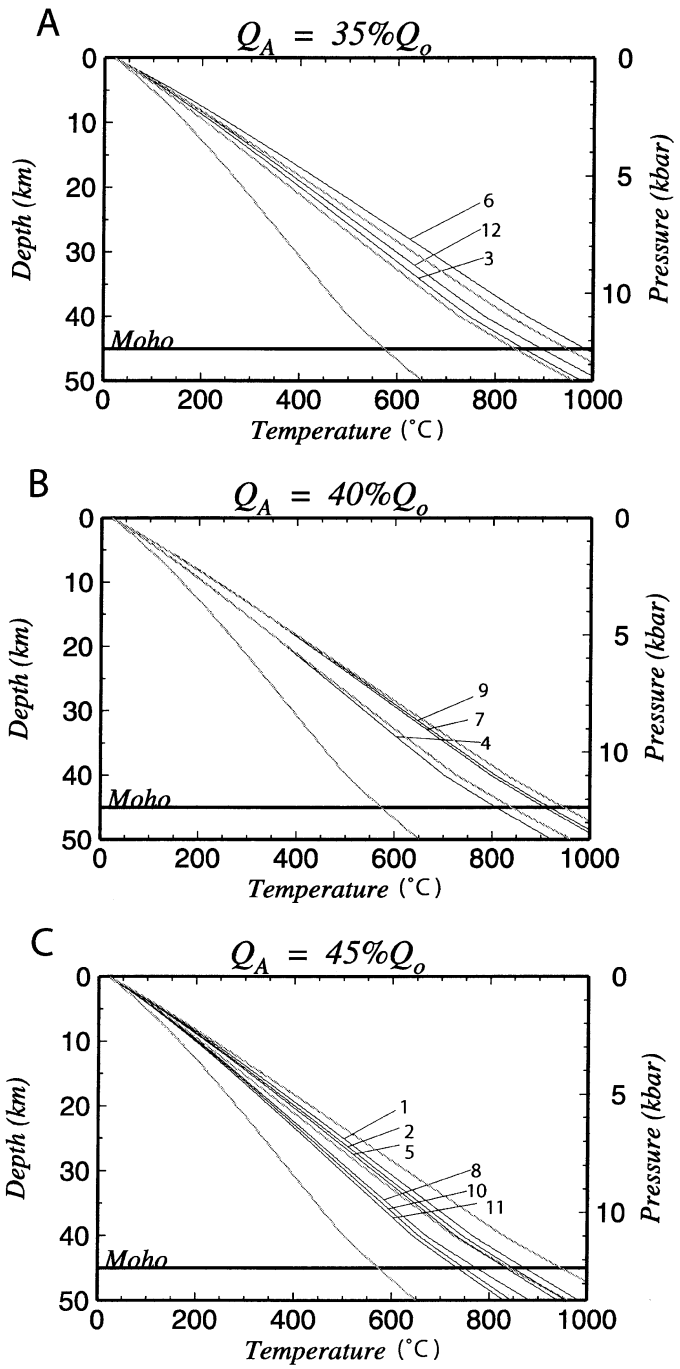

Figure 7. The final 12 geotherms obtained from 72 sets of geotherms in the thermal-parameter sensitivity test. The variables include radiogenic heat flow, scale depth, present surface heat production, mantle heat flow, and erosion time period as mentioned in the text. The solid lines are the final 12 geotherms. Table 5 shows the thermal parameters used in these 12 geotherms.

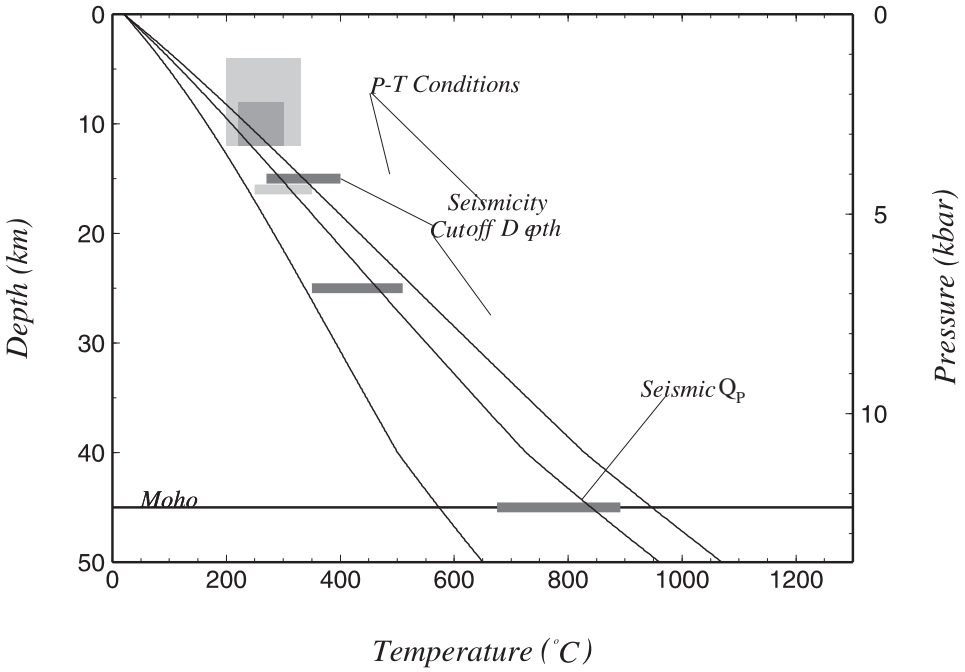

Figure 8. Comparison between the final preferred geotherm with *P-T* conditions determined by metamorphic facies (Chen and Wang, 1995), seismicity cutoff depth, and seismic Q_p (Song, 1997).

optimum results (calculations based on Q_L and D pairs A and C). The geotherm evolution since the initiation of erosion at 5 Ma and 3 Ma is shown in Figure 9, A and B, respectively. The blocking temperatures of apatite (~135 °C) and zircon (~235 °C) are represented by dotted lines. Figure 9A, for the erosion time period beginning at 5 Ma, shows that the exhumation rates corresponding to rock A and rock B are about 1.8 and 2.4 km/m.y., respectively. This exhumation rate is comparable with the exhumation rate of 0.3–2 km/m.y. in the Central Range obtained from the analysis of zircon fission-track data (Tsao, 1996). However, the maximum temperatures that rock A and rock B have undergone are merely ~110 °C and 130 °C, respectively, for the erosion time period beginning at 5 Ma. At their burial depths, neither of them is consistent with the blocking temperature of apatite and zircon and their cooling ages of 0.5 Ma and 2 Ma (Liu, 1982). A similar result could be seen in Figure 9B for the erosion time period of 3 Ma and exhumation rate of 3 and 4 km/m.y. for rock A and rock B, respectively. A deeper burial depth is necessary to satisfy the geochronologic evidence. The temperature in shallow crust seems a little underestimated, especially at a depth of less than 8 km. The principal reasons for the inconsistencies in the shallow crust are, probably, the assumption of constant erosion and exhumation rate and the whole-crust homogeneous thickening. Actually, the exhumation rate is getting faster in the Central Range (Liu, 1982, 1988; Teng, 1990; Tsao, 1996). If true, the real geotherm should slightly increase first and subsequently increase significantly. In addition, the whole-crust homogeneous-thickening model might not be adequate for shallow crust owing to its heterogeneity. Rocks usually deform brittlely in the shallow crust and ductilely in the middle and lower crust. Therefore, the whole-crust homogeneous thickening might be more adequate for the middle and lower crust because of their different rheological characteristics compared to the shallow crust. Instead of the whole-crust homogeneous-thickening model as in this study, for further study, a new model considering crustal thickening by thrusting above the brittle-to-ductile transition (Sibson, 1984) in the shallow crust, and homogeneous thickening in the middle and lower crust might be more appropriate. However, overall, the estimated average geotherm evaluation in the Central Range is considered satisfactory for the middle and lower crust.

In addition, as stated regarding the groundwater-circulation calculation, the anomalously high heat-flow values in the Central Range could be explained by the upward movement of groundwater. The purpose of the heat-flow measurements of Lee and Cheng (1986), in fact, was for hot-spring detection. The depths of those drilled holes are less than 150 m. For the shallow depth, local upward or downward movement of groundwater might have significant effects on the surface heat flow.

The moderate geothermal gradient inferred from our study beneath the Central Range suggests that temperature may not be the only factor responsible for the observed low seismic velocity and low seismicity in the middle and lower crust. Song (1997) has shown that a compositional difference could be responsible for the seismic velocity contrasts observed in the middle and lower crust between the Central Range and Coastal Plain–Western Foothills. Song (1997) adopted the composition and the thermal structure of the current study to construct the rheological structure and calculated the brittle-to-ductile behavior corresponding to the Central Range and Coastal Plain–Western Foothills. His results show that the seis-

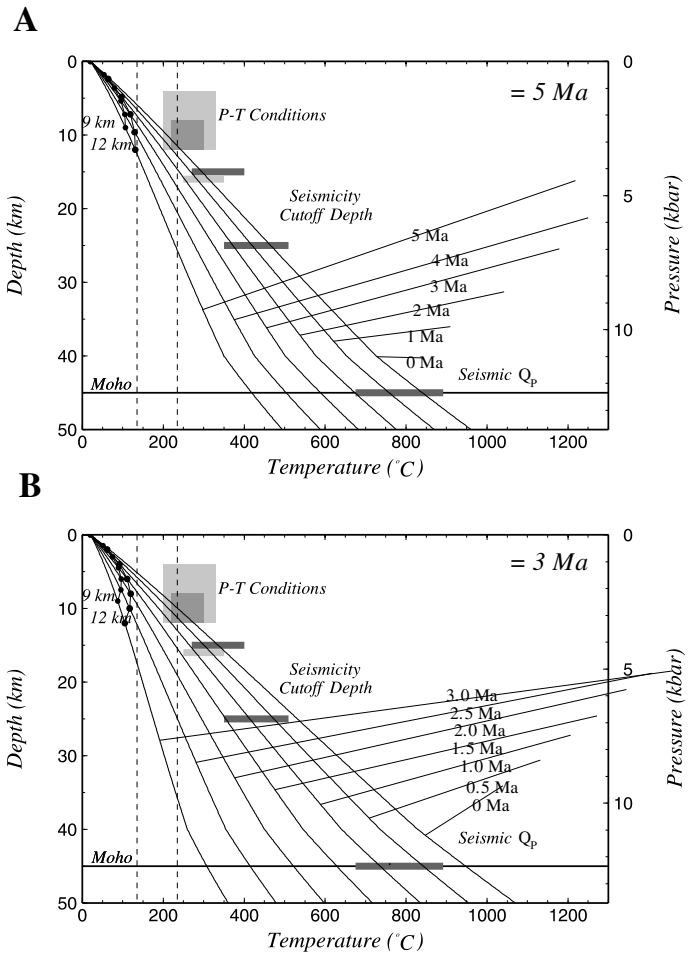

Figure 9. The geotherm evolution and *P-T-t* path derived in our study. (A) Geotherm evolution in 1 m.y. time intervals, considering a constant erosion rate since 5 Ma ($\lambda = 5$). (B) Geotherm evolution in 0.5 m.y. time intervals, considering a constant erosion rate since 3 Ma ($\lambda = 3$). Two vertical dashed lines represent the blocking temperature of 135 °C and 235 °C of apatite and zircon, respectively. Calculated *P-T-t* paths of rocks A and B initially buried at the depths of 9 km and 12 km are represented by dots. The depth of the Moho represents the present crustal thickness of ~45 km, denoted by horizontal thick lines.

micity of these two provinces can be satisfactorily explained by their brittle-to-ductile behavior. It suggests that the seismicity pattern and velocity beneath the Central Range might be controlled by not only temperature, but also by composition. A high geothermal gradient or temperature is not required for these apparent geophysical observations.

CONCLUSIONS

The thermal structure beneath the Central Range, Taiwan, has been estimated on the basis of the whole-crustal homogeneous-thickening model. Geotherms were calculated by considering as steady state the crustal radiogenic and mantle heat flow, whereas the ongoing tectonic collision provides a transient effect on the present geotherm. Groundwater circulation is considered to explain anomalously high and low heat flows. The transient factors of crustal thickening, uplift, and erosion have significant contributions to the geotherms. The crustal thickening results in a decrease of the temperature; the exhumation results in an increase of the temperature. The preferred final geotherm thus estimated has a geothermal gradient of ~17 °C/km in the middle and lower crust. Because most of the thermal parameters used in the geotherm calculation are subject to uncertainties owing to lack of available data, the sensitivity of our final geotherm calculation to the assumed geotherm parameters are examined. The sensitivity study shows that the parameters used in the final geotherm calculations are reasonable. The effects of the alternative geotherm parameters on the final geotherms are within the range of our estimated preferred geotherm. The preferred final geotherm is comparable with the temperature derived from the observed depth of seismic cutoff (i.e., the depth to the brittle-to-ductile transition depth) and seismic attenuation Q_p. However, the temperature at the shallow crust is not consistent with *P-T* conditions observed in the Central Range because of the assumption of constant erosion rate and exhumation rate in our model. Simulations of groundwater circulation show that the anomalous heat-flow values probably result from the upward and downward movement of groundwater. Crustal thickening plays an important role in the Taiwan orogeny. The moderate geothermal gradient and temperatures beneath the Central Range suggest to us that temperature might not be the only factor causing the observed lack of seismicity and seismic velocity in the Central Range.

ACKNOWLEDGMENTS

We thank reviewers B.-Y. Kuo, J.-H. Wang, and W.D. Mooney. Discussions with C.-H. Lo, F. Wu, and C.-Y. Wang were very helpful. This work was supported by NSC89-2119-M-008-001.

REFERENCES CITED

Artemieva, I.M. and Mooney, W.D., 2001 Thermal thickness and evolution of Precambrian lithosphere: A global study: Journal of Geophysical Research, v. 106, p. 16 387–16 414.

Barr, T.D., and Dahlen, F.A., 1989, Brittle frictional mountain building. 2. Thermal structure and heat budget: Journal of Geophysical Research, v. 94, p. 3923–3947.

Batt, T.D., and Braun, J., 1997, On the thermomechanical evolution of compressional orogens: Geophysical Journal International, v. 128, p. 364–382.

Bordi, B., and Iizuka, S., 1993, Thermal regime, rheology, and seismicity in Central Range: Tectonophysics, v. 217, p. 1–9.

Chang, H.C., 1989, Radioactivity and heat generation of rocks in the Taiwan region (in Chinese) [Ph.D. thesis]: Chung-Li, National Central University, 159 p.

Chen, C.H., and Wang, C.H., 1995, Explanatory notes for the metamorphic facies map of Taiwan (in Chinese), (second edition): Central Geological Survey Special Publication, 51 p.

Chen, C.H., 1989, Hot springs and geotherm heat in Taiwan (in Chinese): *Ti-Chih*, v. 9, p. 327–340.

Chen, K.J., Yeh, Y.H., and Shyu, C.T., 1996, Qp structure in the Taiwan area and its correlation to seismicity: TAO, Terrestrial, Atmospheric and Oceanic Sciences, v. 7, p. 409–429.

Doser, D.I., and Kanamori, H., 1986, Depth of seismicity in the Imperial Valley region (1977–1983) and its relationship to heat flow, crustal temperature, and the October 15, 1979, earthquake: Journal of Geophysical Research, v. 91, p. 675–788.

Elder, J.W., 1965, Physical processes in geothermal areas, *in* Lee, W.H.K., ed., Terrestrial heat flow: American Geophysical Union Geophysical Monograph 8, p. 211–235.

England, P.C., 1978, Some thermal considerations of the Alpine metamorphism: Past, present and future: Tectonophysics, v. 46, p. 21–40.

England, P.C., and Thompson, A.B., 1984a, Pressure-temperature-time paths of regional metamorphism. 1. Heat transfer during the evolution of regions of thickened continental crust: Journal of Petrology, v. 25, p. 894–928.

England, P.C., and Richardson, S.W., 1980, Erosion and the age dependence of continental heat flow: Geophysical Journal of the Royal Astronomical Society, v. 62, p. 421–437.

Haack, U., 1983, On the content and vertical distribution of K, Th, and U in the continental crust: Earth and Planetary Science Letters, v. 62, p. 360–366.

Ho, C.S., 1982, Tectonic evolution of Taiwan and explanatory text of the tectonic map of Taiwan: Taipei, Taiwan, Republic of China, Central Geological Survey, Ministry Economic Affairs, 126 p.

Ho, C.S., 1988, An introduction to the geology of Taiwan and explanatory text of the geologic map of Taiwan: Taipei, Taiwan, Republic of China, Central Geological Survey, Ministry of Economic Affairs, 192 p.

Hsu, S.K., and Sibuet, J.C., 1995, Is Taiwan the result of arc-continent or arc-arc collision?: Earth and Planetary Science Letters, v. 136, p. 315–324.

Huerta, A.D., Royden, L.H., and Hodges, K.V., 1996, The interdependence of deformation and thermal process in mountain belts: Science, v. 273, p. 637–642.

Huerta, A.D., Royden, L.H., and Hodges, K.V., 1998, The thermal structure of collision orogens as a response to accretion, erosion, and radiogenic heating: Journal of Geophysical Research, v. 103, p. 15287–15302.

Hwang, C.Y., Wu, W.Y., Chang, C.P., Tsao, S., Yuan, P.B., Lin, C.W., and Yuan, X.K., 1997, Tectonic evolution of accretionary prism in the arc-continental collision terrane of Taiwan: Tectonophysics, v. 281, p. 31–51.

Hwang, W. T., and Wang, C.Y., 1993, Sequential thrusting model for mountain building: Constraints from geology and heat flow of Taiwan: Journal of Geophysical Research, v. 98, p. 9963–9973.

Lachenbruch, A.H., and Sass, J.H., 1977, Heat flow in the United States and the thermal regime of the crust, *in* Heacock, J.G., ed., The earth's crust: Its nature and physical properties: American Geophysical Union Geophysical Monograph 20, p. 626–675.

Lachenbruch, A.H., 1970, Crustal temperature and heat production: Implications of the linear-flow relation: Journal of Geophysical Research, v. 75, p. 3291–3300.

Lachenbruch, A.H., Sass J.H., Clow, G.D., and Weldon, R., 1995, Heat flow at Cajon Pass, California, revisited: Journal of Geophysical Research, v. 100, p. 2005–2012.

Lamontagne, M., and Ranalli, G., 1996, Thermal and rheological constraints on the earthquake depth distribution in the Charlevoix, Canada, intraplate seismic zone: Tectonophysics, v. 257, p. 55–69.

Lan, C.Y., Lee, T., and Lee, C.W., 1990, The Rb-Sr isotope record in Taiwan gneiss and its tectonic implication: Tectonophysics, v. 183, p. 129–143.

Lee, S.J., 1999. The S-wave velocity structure under center-west Taiwan by string ground motion waveform modeling (in chinese) [M. S. thesis]: Chung-Li, National Central University, 138 p.

Lee, C.R., and Cheng, W.T., 1986, Preliminary heat flow measurement in Taiwan: Proceedings, 4th Circum-Pacific Energy and Mineral Resources Conference, Singapore, p. 31–36.

Liu, T.K., 1982, Tectonic implication of fission track ages from the Central Range, Taiwan: Proceedings of the Geological Society of China, no. 25, p. 22–37.

Liu, T.K., 1988, Fission-track dating of Hsueshan Range: Thermal record due to arc-continent collision in Taiwan: Acta Geolologica Taiwanica, v. 26, p. 279–290.

Lo, C.H., and Yui, T.F., 1996, $^{40}Ar/^{39}$ Ar dating of high-pressure rocks in the Tananao basement complex, Taiwan: Journal of the Geological Society of China, v. 39, p. 13–30.

Lu, C.Y., and Hsu, K.J., 1992, Tectonic evolution of the Taiwan mountain belt: Petroleum Geology of Taiwan, v. 27, p. 21–46.

Ma, K.F., and Song, T.R., 1997, Pn velocity and Moho depth in Taiwan: Journal of the Geological Society of China, v. 40, p. 167–184.

Ma, K.F., Wang, J.H., and Zhao, D., 1996, Three-dimensional seismic velocity structure of the crust and uppermost mantle beneath Taiwan: Journal of Physics of the Earth, v. 44, p. 85–105.

Mancktelow, N.S., and Graseman, B., 1997, Time-dependent effects of heat advection and topography on cooling histories during erosion: Tectonophysics, v. 270, p. 167–195.

Meissner, R., 1986, The continental crust: A geophysical approach: Orlando, Florida, Academic Press, Inc., p. 361–362.

Mishra, D.C., 1982, Crustal structure and dynamics under Himalaya and Pamir ranges: Earth and Planetary Science Letters, v. 57, p. 415–420.

Morgan, P., and Gosnold, W.D., 1989, Heat flow and thermal regimes in the continental crust, *in* Pakiser, L.C., and Mooney, W.D., eds., Geophysical framework of the Conterminous United States: Geological Society of America Memoir 172, p. 493–522.

Ord, A., and Hobbs, B.E., 1989, The strength of the continental crust, detachment zones and the development of plastic instabilities: Tectonophysics, v. 158, p. 269–289.

Pollack, H.N., and Chapman, D.S., 1977, On the regional variation of heat flow, geotherms and lithospheric thickness: Tectonophysics, v. 38, p. 279–296.

Prodehl, C., and Pakiser, L.C., 1980, Crustal structure of the southern Rock Mountains from seismic measurements: Geological Society of America Bulletin, v. 91, p. I147–I155.

Rau, R.J., and Wu, F.T., 1995, Tomographic imaging of lithospheric structures under Taiwan: Earth and Planetary Science Letters, v. 133, p. 517–532.

Richardson, S.W., and England, P.C., 1979, Metamorphic consequences of crustal eclogite production in overthrust orogenic zones: Earth and Planetary Sciences Letters, v. 42, p. 183–190.

Rodgers, A.J., and Schwartz, S.Y., 1997, Low crustal velocities and mantle lithospheric variation in southern Tibet from regional Pnl waveforms: Geophysical Research Letters, v. 24, p. 9–12.

Rudnick, R.L., 1992, Restites, Eu anomalies, and the lower continental crust: Geochimica et Cosmochimica Acta, v. 56, p. 963–970.

Rybach, L., and Cermak, V., 1982, Radioactive heat generation in rocks, *in* Angenheister, G., ed., Physical Properties of Rocks, Numerical data and functional relationships in sciences and technology, New Series, Group 5, Volume 1a: Landolt-Bornstein, Berlin, Springer Verlag, p. 353–371.

Sato, H., 1994, H_2O and magmatism in island arc mantle inferred from seismic anelasticity and heat flow data: Journal of Physics of the Earth, v. 42, p. 439–453.

Sato, H., and Sacks, I.S., 1989, Anelasticity and thermal structure of the oceanic upper mantle: Temperature calibration with heat flow data: Journal of Geophysical Research, v. 94, p. 5705–5715.

Sclater, J. Jaupart, G.C., and Galson, D., 1980, The heat flow through oceanic and continental crust and the heat loss of the earth: Reviews of Geophysics, v. 18, no. 1, p. 269–311.

Shih, R.C., Lin, C.H., Lai, H.L., Yeh, Y.H., Huang, B.B., and Yen, H.Y., 1998, Preliminary crustal structures across central Taiwan from modeling of the

onshore-offshore wide-angle seismic data: TAO, Terrestrial, Atmospheric, and Oceanic Sciences, v. 9, p. 317–328.
Sibson, R.H., 1982, Fault zone models, heat flow, and the depth distribution of earthquakes in the continental crust of the United States: Bulletin of the Seismological Society of America, v. 72, p. 151–163.
Sibson, R.H., 1984, Roughness at the base of the seismogenic zone: Contributing factors: Journal of Geophysical Research, v. 89, p. 5791–5799.
Song, T.-R.A., 1997, Characteristics of continental crust in Taiwan orogenic belts (in Chinese) [M.S. thesis]: Chung-Li, National Central University, 134 p.
Stuwe, K., White, L., and Brown, R., 1994, The influence of eroding topography on steady-state isotherms: Application to fission track analysis: Earth and Planetary Science Letters, v. 124, p. 63–74.
Suppe, J., 1980, A retrodeformable cross-section of northern Taiwan: Proceedings of the Geological Society of China, v. 23, p. 46–55.
Takahashi, E., 1986, Melting of a dry peridiotite KLB-a up to 14 Gpa: Implications on the origin of peridotitic upper mantle: Journal of Geophysical Research, v. 91, p. 9367–9382.
Teng, L.S., 1990, Geotectonic evolution of late Cenozoic arc-continental collision in Taiwan: Tectonophysics, v. 183, p. 57–76.
Toksoz, M.N., and Bird, P., 1977, Modeling of temperature in continental convergence zones: Tectonophysics, v. 41, p. 181–193.
Tsai, Y.B., 1986, Seismotectonics in Taiwan: Tectonophysics, v. 125, p. 17–38.
Tsao, S., 1996, The geological significances of illite crystallinity, zircon fission-track ages, and K-Ar ages of metasedimentary rocks of the Central Range of Taiwan [Ph.D. thesis]: Taipei, National Taiwan University, 272 p.
Vitorello, I., and Pollack, H.N., 1980, On the variation of continental heat flow age and the thermal evolution of continents: Journal of Geophysical Research, v. 85, p. 983–995.
Volvovsky, B.S., Volvovsky, I.S., and Kambarov, N.S., 1983, Geodynamics and seismicity of the Pamir-Himalaya region: Physics of the Earth and Planetary Interiors, v. 31, p. 307–312.
Wang, J.H., and Chen, K.C., and Lee, T.Q., 1994, Depth distribution of shallow earthquakes in Taiwan: Journal of the Geological Society of China, v. 37, p. 125–142.
Wu, F.T., 1978, Recent tectonics of Taiwan: Journal of Physics of the Earth, v. 26, p. s265–s299.
Wu, F.T., Rau, R.J., and Salzberg, D., 1997, Taiwan orogeny: Thin-skinned or lithospheric collision?: Tectonophysics, v. 274, p. 191–220.

Appendix

For a circulation depth of ~4 km (Elder, 1965; Lachenbruch and Sass, 1977; Chen, 1989), from a simple idealized one-dimensional model for groundwater circulation, the temperature at the circulation depth due to the groundwater circulation can be estimated (Lachenbruch and Sass, 1977) as

$$T(t) = T(0) - T(0)[1 - (1/N)][1 - e^{-\beta 2}\ \mathrm{erfc}(\beta)], \quad \text{(A-1)}$$

where $T(0)$ is the temperature at the bottom of the circulated depth ($h = 4$ km) whereas the groundwater effect has not yet been taken into account. $\beta = [(N^2\alpha)/h^2]t$, and N has the form

$$N = \tfrac{1}{2}(e^{h/|s|} + e^{-h/|s|}), \quad \text{(A-2)}$$

by assuming a layer with uniform vertical flow, upward over half the area and downward over the other half. As $t \approx h^2/(N^2\alpha)$, termed the "stabilization time" t_W, $T(t = t_W)$ will approach the equilibrium temperature $T(0)/N$.

Table A-1 lists the corresponding stabilization times t_W and equilibrium temperatures for various groundwater velocities. For the circulation depth of 4 km assumed in this study, Lachenbruch and Sass (1977) suggested the stabilization time should be on the order of about 10^5 yr. As listed in Table A-1, for the velocity of 0.0075 m/yr, the corresponding stabilization time t_W is about 130 000 yr, which is on the order of magnitude 10^5. We consider the groundwater velocity of 0.0075 m/yr as the appropriate velocity in our study.

Manuscript Accepted by the Society